AMBIGUITY ANALYSIS AND THE CONSTRAINED INVERSION OF POTENTIAL FIELD DATA

Fabio Boschetti
Franklin G. Horowitz
Peter Hornby

Australian Geodynamics Cooperative Research Centre
and
CSIRO Exploration & Mining
39 The Fairway (P.O. Box 437)
Nedlands, Western Australia 6009

ABSTRACT

Given a Poisson potential field (or its derivatives) on a plane in free space, the entire ambiguity domain (i.e., the set of all source distributions that could generate the field) is easily reconstructed in the Fourier domain. The resulting models show a range of variability far larger than normally expected. In essence, potential fields in free space only contain enough information to determine an equivalent layer source. Anything further must be supported by *a priori* information. We formulate an inverse problem as a search in the set of all compatible source distributions for solutions that also satisfy hard constraints, such as downhole data and trusted cross-sections, and soft constraints in the form of statistical information. Our experiments show that statistical information is particularly effective in guiding the search towards solutions resembling the regional geological style. A limited amount of hard information in the form of drillholes appears to be required to reduce the translational freedom admitted by the statistical characterisation.

1   Introduction

Among the different techniques available in exploration geophysics to obtain information about the distribution of material underground, the analysis of potential field data is of major interest. It is relatively inexpensive, and airborne surveys allow the coverage of large, sometimes inaccessible, areas.

It follows that the literature on the inversion of potential field data is very rich. Blakely (1995) presents an accessible overview. We broadly divide the methods currently available into three categories, model-free, assumed source, and 'image processing based' methods. In model-free methods, the region of interest is discretised into regular blocks of constant density (for gravity surveys) or magnetisation/susceptibility (for magnetic surveys), and the problem reduces to finding a distribution of material that satisfies the observations in a least squares sense. The principle of linear superposition

1

applies to the calculation of the field, and so these methods are sometimes called 'linear methods'.

In assumed source models, the unknown bodies are typically described with simple, regular shapes such as spheres, polyhedra, thin layers, etc. The geometrical parameters of these shapes, together with their locations, are the target of the inversion. The equations determining these parameters are generally non-linear, hence the nomenclature 'non-linear methods' is sometimes applied.

A number of methods are also available for a fast analysis of large data sets. They are used to determine the average location of the main anomalous bodies under a number of quite strict assumptions. Examples include Euler deconvolution methods (Thompson, 1982), Werner deconvolution methods (Ku and Sharp, 1983), the analytic signal approach (Roest, Verhoef and Pilkington, 1992), Spector and Grant's (1970) 'statistical' approach and similar methods (Blakely and Simpson, 1986; Miller and Singh, 1994). These methods have a character of image processing (or migration algorithms in reflection seismic processing), though the boundary between these methods and our other two classes is somewhat arbitrary.

No matter which method one employs, the inversion of potential field data is always non-unique. An infinite number of solutions can be found that satisfy the data equally well. This problem is usually circumvented by looking for solutions with unique features (for example, searching for the smoothest distribution of material satisfying the data), thus forcing an non-unique problem to behave as a unique one. However, this leaves the actual extent of the ambiguity domain (i.e., the range of variability of the solutions to a potential field inverse problem) unknown. Worse, the ambiguity is disguised by these methods. This issue affects both the implementation of the inverse problem and the interpretation of its results. In particular it prevents us from answering the following questions. How much does the problem parameterisation affect the final results? Given a solution to the problem, is there another solution that would lead to a completely different geological interpretation? Is there a solution that can capture the average features of the ambiguity domain? Basically, this is an issue of reliability of the overall inversion process.

Answers to some of these questions can be found in the literature. Parker (1974, 1975) showed how it is possible to define the admissible bounds of density values consistent with a set of gravity measurements. As these bounds are a function of depth, one can estimate the likelihood of simple sources characterised by certain density values at different depths. Ander and Huestis (1987) and Huestis and Parker (1977) performed similar studies relating density/susceptibility values to the thickness of the causative bodies. Al-Chalabi (1971) attempted to describe the ambiguity domain by exhaustive sampling of small 2-D portions of the entire space. Because of the limitations

in parameterisation, the actual size of the ambiguity was underestimated. Also in the spirit of describing the ambiguity domain, Vasco, Johnson and Majer (1993) and Boschetti, Dentith and List (1997), attempted an analysis of sets of possible solutions using statistical means, to determine the variance and the bounds on the parameters for acceptable solutions and possibly recover an average model representative of the entire set. These approaches suffer from the limitation that the extent of the ambiguity domain is so large, and its shape so complicated, that reasonable results may be obtained only for very simple problems. Also, Vasco's and Boschetti's methods perform the statistical analysis on the collection of solutions found via specific inversion algorithms. Despite the size of this collection being large compared to that obtainable with traditional inversion methods, the question remains whether their specific algorithms sample the solution space uniformly.

In a more formal approach, Mareschal (1985) proposed a technique to reconstruct the entire ambiguity domain (the space of all possible solutions that *exactly* satisfy the observations). The method works by finding a complete set of orthogonal functions spanning the ambiguity domain. Any solution satisfying the data can then be obtained from this set of functions. However, the formulation proposed by Mareschal makes use of Laguerre polynomials, which leads to a parameter space difficult to relate to geometry and geology.

In this paper we propose a modification to Mareschal's method. We first discretise the source into layers, with constant density/susceptibility across each layer. The horizontal variation within a layer is discretised by point sampling on a regular grid. Thus, we nearly have a 'voxel' representation. However, this is not quite the same as a voxel representation, since the horizontal variation is not piecewise constant, but rather, is a smooth (band limited) function interpolating between the sample points. The vertical variation is, however, piecewise constant. Through simple calculations in the Fourier domain we are able to reconstruct the entire ambiguity domain to potential field inverse problems at a given resolution.

This reconstruction in useful in two ways. First, we can analyse the actual extent of the ambiguity of very simple potential field anomalies. Even though the non-uniqueness of potential field inversions is widely known, a visual appraisal of the range of variability allowed in the solutions may be striking. We present a few examples to caution against the rote use of inversion techniques that might lead to largely erroneous solutions.

Second, we can employ such reconstruction in an inverse approach. When the entire ambiguity domain has been suitably described, particular solutions can be selected using *a priori* information. The idea is to implement an algorithm able to make use of any available information, such as downhole samples, geological cross-sections, seismic profiles, statistical information (e.g. geological styles or textures typical of the area) and so on. One selects a

suitable model by performing a global search in the ambiguity domain. The search finds high probability solutions by minimising some cost function designed to appropriately balance the different kinds of *a priori* information available. Only solutions that **exactly** satisfy the potential field data are considered in the search.

2   Direct Inversion of Potential Field Data

In this section, under the 'flat earth' approximation, we present the basic formulae employed in the reconstruction of the ambiguity domain for both gravity and magnetic inversion.

2.1   Gravitational Acceleration

The scalar potential energy V at a point (x, y, z) due to a mass density $\rho(x, y, z)$ is given by

$$V(x, y, z) = -G \int_{\Re^2} dx' dy' \int_{-\infty}^{0} \frac{\rho(x', y', z')}{\left((x - x')^2 + (y - y')^2 + (z - z')^2\right)^{1/2}} \, dz' \qquad (2.1)$$

where G is the gravitational constant, and the resulting acceleration vector is $-\nabla V$. We take z to be positive upwards, and assume that $\rho(x, y, z) = 0$ for $z > 0$. The magnitude of vertical acceleration at (x, y, z) (negative of the vertical component) is given by

$$f_z(x, y) = \frac{\partial V}{\partial z} = G \int_{\Re^2} dx' dy' \int_{-\infty}^{0} \frac{\rho(x', y', z')(z - z')}{((x - x')^2 + (y - y')^2 + (z - z')^2)^{3/2}} dz'. \qquad (2.2)$$

Equation (2.2) has the form of a 2 dimensional convolution

$$f_z(x, y) = 2\pi G \int_{-\infty}^{0} \rho(x, y, z') * \gamma_{z-z'}(x, y) dz' \qquad (2.3)$$

where $(*)$ is the 2-D convolution in (x, y) and

$$\gamma_z(x, y) = \frac{1}{2\pi} \frac{z}{(x^2 + y^2 + z^2)^{3/2}} \qquad (2.4)$$

is the Green's function for vertical acceleration. Define a 2-D Fourier transform (and its inverse) in the (x, y) plane as

$$\hat{f}(\mathbf{k}) = \Im[f] = \int_{\Re^2} f(\mathbf{x})\exp(-2\pi i\mathbf{k}\cdot\mathbf{x})d\mathbf{x}$$

$$f(\mathbf{x}) = \Im^{-1}\left[\hat{f}\right] = \int_{\Re^2} \hat{f}(\mathbf{k})\exp(2\pi i\mathbf{k}\cdot\mathbf{x})d\mathbf{k}$$

(2.5)

where boldface denotes a 2-D vector. We then have (e.g. Bracewell, 1965 or Bhattacharyya, 1966)

$$\hat{\gamma}_z(k_x,k_y) = \exp(-2\pi\|\mathbf{k}\|z) \qquad z > 0.$$

(2.6)

Applying the convolution theorem to Equation (2.3) yields

$$\hat{f}_z(k_x,k_z) = 2\pi G\int_{-\infty}^{0}\hat{\rho}(k_x,k_y,z')\hat{\gamma}_{z-z'}(k_x,k_y)dz'.$$

(2.7)

Now suppose that we want to calculate the vertical acceleration of a flat layer parallel to the surface between $z' = z_1$ and $z' = z_2$, whose density varies only in horizontal directions. The resulting integral is

$$\hat{f}_z(k_x,k_z) = 2\pi G\,\hat{\rho}(k_x,k_y)\int_{z_1}^{z_2}\hat{\gamma}_{z-z'}(k_x,k_y)dz'.$$

(2.8)

Hence, we obtain for the transform of the vertical acceleration of the flat layer

$$\hat{f}_z(\mathbf{k}) = \hat{g}_z(\mathbf{k})\hat{\rho}(\mathbf{k})$$

(2.9)

where $\hat{\rho}$ is the Fourier transform of the horizontal density variation and

$$\hat{g}_z(\mathbf{k}) = \frac{G}{\|\mathbf{k}\|}\left\{\exp(2\pi\|\mathbf{k}\|z_2) - \exp(2\pi\|\mathbf{k}\|z_1)\right\}\exp(-2\pi\|\mathbf{k}\|z)$$

(2.10)

is the 'layer source influence function'. We refer the interested reader to Blakely (1995) for a different formulation.

2.2 Total Magnetic Field Anomaly

For static magnetic fields, the scalar magnetic potential at a point $\vec{x} = (x,y,z)^{\mathrm{T}}$ due to an anomalous dipole moment distribution $\vec{m}(\vec{x})$ (where $\vec{a}$ denotes a 3-D vector) is given by

$$V(\vec{\mathbf{x}}) = C \int_{\Re^2} dx'dy' \int_{-\infty}^{0} \vec{\mathbf{m}}(\vec{\mathbf{x}}') \cdot \nabla' \left((x-x')^2 + (y-y')^2 + (z-z')^2 \right)^{-1/2} dz'$$

$$= C \int_{\Re^2} dx'dy' \int_{-\infty}^{0} \vec{\mathbf{m}}(\vec{\mathbf{x}}') \cdot \nabla \left(-r^{-1} \right) \Big|_{\vec{\mathbf{x}}-\vec{\mathbf{x}}'} dz' \qquad (2.11)$$

where C is 1 in *emu* or $\mu_0/4\pi$ in S.I. units and ∇' denotes the gradient with respect to primed coordinates. We again take z to be positive upwards, and suppose that $\vec{\mathbf{m}}(x,y,z) = \mathbf{0}$ for $z > 0$. The resulting anomalous magnetic field $\vec{\mathbf{B}} = -\nabla V$.

Under the (usual) twin assumptions that the magnetic field due to the anomaly is small compared to the ambient field $\vec{\mathbf{F}}$, and that the ambient field does not change direction over the survey, the scalar total field anomaly is harmonic, and given by (to first order in the anomaly field; e.g. Blakely, 1995)

$$f_z(x,y) = \vec{\mathbf{e}}_{\mathbf{F}} \cdot \vec{\mathbf{B}} = \vec{\mathbf{e}}_{\mathbf{F}} \cdot \left(-\nabla V(\vec{\mathbf{x}}) \right)$$

$$= -C \int_{\Re^2} dx'dy' \int_{-\infty}^{0} \vec{\mathbf{e}}_{\mathbf{F}} \cdot \nabla \left(\vec{\mathbf{m}}(\vec{\mathbf{x}}') \cdot \nabla' \left(\|\vec{\mathbf{x}} - \vec{\mathbf{x}}'\|^{-1} \right) \right) dz' \qquad (2.12)$$

where $\vec{\mathbf{e}}_{\mathbf{F}}$ is a 3-D unit vector in the direction of $\vec{\mathbf{F}}$. The integral in Equation (2.12) over x' and y' has the form of a two dimensional convolution. Proceeding cautiously regarding whether the gradients are evaluated at the observation point (∇) or the source point (∇'), (noting that $\nabla' = -\nabla$ when applied to the convolution kernel) we find that

$$\Im\left[\nabla' \|\vec{\mathbf{x}} - \vec{\mathbf{x}}'\|^{-1} \right] = \begin{pmatrix} -2\pi i k_x \\ -2\pi i k_y \\ \frac{\partial}{\partial z'} \end{pmatrix} \frac{\exp\left(-2\pi \|\mathbf{k}\|(z-z') \right)}{\|\mathbf{k}\|}$$

$$= 2\pi \begin{pmatrix} -i k_x \\ -i k_y \\ \|\mathbf{k}\| \end{pmatrix} \frac{\exp\left(-2\pi \|\mathbf{k}\|(z-z') \right)}{\|\mathbf{k}\|} \qquad (2.13)$$

Taking the two dimensional Fourier transform of Equation (2.12) together with Equation (2.13) yields

$$\hat{f}_z = -4\pi^2 C \int_{-\infty}^{0} \vec{\mathbf{e}}_{\mathbf{F}} \cdot \begin{pmatrix} i k_x \\ i k_y \\ -\|\mathbf{k}\| \end{pmatrix} \left(\hat{\vec{\mathbf{m}}}(k_x, k_y, z') \cdot \begin{pmatrix} -i k_x \\ -i k_y \\ \|\mathbf{k}\| \end{pmatrix} \right) \frac{\exp\left(-2\pi \|\mathbf{k}\|(z-z') \right)}{\|\mathbf{k}\|} dz'. \qquad (2.14)$$

Writing the product of the two factors corresponding to $\vec{\mathbf{e}}_F \cdot \nabla$ and $\vec{\mathbf{m}} \cdot \nabla'$ as an outer product, we find

$$\hat{f}_z = -4\pi^2 C \int_{-\infty}^{0} \vec{\mathbf{e}}_F^T \left(\begin{pmatrix} ik_x \\ ik_y \\ -\|\mathbf{k}\| \end{pmatrix} \otimes \begin{pmatrix} -ik_x & -ik_y & \|\mathbf{k}\| \end{pmatrix} \right) \hat{\vec{\mathbf{m}}}(\mathbf{k}, z') \frac{\exp\left(-2\pi\|\mathbf{k}\|(z-z')\right) dz'}{\|\mathbf{k}\|}$$

$$= -4\pi^2 C \vec{\mathbf{e}}_F^T \vec{\Lambda}(\mathbf{k}) \int_{-\infty}^{0} \hat{\vec{\mathbf{m}}}(\mathbf{k}, z') \frac{\exp\left(-2\pi\|\mathbf{k}\|(z-z')\right)}{\|\mathbf{k}\|} dz'$$

(2.15)

where the tensor operator $\vec{\Lambda}$ is (in the Fourier domain) the matrix

$$\vec{\Lambda}(\mathbf{k}) = \begin{pmatrix} k_x^2 & k_x k_y & ik_x\|\mathbf{k}\| \\ k_x k_y & k_y^2 & ik_y\|\mathbf{k}\| \\ ik_x\|\mathbf{k}\| & ik_y\|\mathbf{k}\| & -\|\mathbf{k}\|^2 \end{pmatrix} .$$

(2.16)

Suppose again that we want to calculate the field of a flat layer parallel to the surface between $z' = z_1$ and $z' = z_2$, whose magnetisation varies only in horizontal directions. We obtain as the transform of the total field anomaly due to the flat layer,

$$\hat{f}_z = -4\pi^2 C \vec{\mathbf{e}}_F^T \vec{\Lambda}(\mathbf{k}) \hat{\vec{\mathbf{m}}}(\mathbf{k}) \int_{z_1}^{z_2} \frac{\exp\left(-2\pi\|\mathbf{k}\|(z-z')\right)}{\|\mathbf{k}\|} dz'$$

$$= -\frac{2\pi C}{\|\mathbf{k}\|^2} \left\{ \exp\left(-2\pi\|\mathbf{k}\|(z-z_2)\right) - \exp\left(-2\pi\|\mathbf{k}\|(z-z_1)\right) \right\} \vec{\mathbf{e}}_F^T \vec{\Lambda}(\mathbf{k}) \hat{\vec{\mathbf{m}}}(\mathbf{k})$$

(2.17)

where $\hat{\vec{\mathbf{m}}}$ is the 2-D Fourier transform of the magnetisation. If we further assume that the direction of the magnetisation $\vec{\mathbf{m}}$ is constant, $\vec{\mathbf{m}}(\vec{\mathbf{x}}) = m(\vec{\mathbf{x}})\vec{\mathbf{e}}_m$ say, then we obtain the relation between scalar quantities

$$\hat{f}_z(\mathbf{k}) = \hat{g}_z(\mathbf{k})\,\hat{m}(\mathbf{k})$$

(2.18)

where

$$\hat{g}_z(\mathbf{k}) = 2\pi C \left\{ \exp\left(2\pi\|\mathbf{k}\|z_1\right) - \exp\left(2\pi\|\mathbf{k}\|z_2\right) \right\} \frac{\vec{\mathbf{e}}_F^T \vec{\Lambda}(\mathbf{k})\vec{\mathbf{e}}_m}{\|\mathbf{k}\|^2} \exp\left(-2\pi\|\mathbf{k}\|z\right)$$

(2.19)

is now the 'layer source influence function' for magnetic fields. Note that the vector-matrix-vector factor in (2.19) reduces to the (complex) scalar quantity that is sometimes written as the product $\theta_m \theta_f$ (e.g. Equation 11.25 in Blakely, 1995), but that (2.17) is more general.

3   Reconstruction of the Ambiguity Domain

In this section we describe how Equations (2.9) or (2.18) can be used to reconstruct the ambiguity domain for a potential field problem. The inversion of potential field data for an equivalent layer source can be written as a deconvolution

$$\Im[S] = \Im[f] / \Im[g] \tag{3.1}$$

where S is the source, f is the measurement and g is the appropriate layer influence function (developed in the previous sections).

Suppose that the data set f contains M measurements regularly sampled in the horizontal direction(s). We will invert for source distributions which are non-zero in the domain $z < 0$. As an aside, f is rarely exhaustively sampled in such a fashion. Rather, it is interpolated to a regular grid from sparse sampling (a form of inversion in itself, e.g. Issaks & Srivastava, 1989; Horowitz et al., 1996). Thus, the spectral content $\Im[f]$ is itself known only within the constraints imposed by this interpolation. For the rest of this paper, we pragmatically neglect this effect and assume that $\Im[f]$ is known perfectly. Clearly, however, there is scope for a more comprehensive inversion constrained explicitly by the actual samples of f (although possibly not implemented within the framework of Fourier transforms).

The source variation is assumed to be piecewise constant vertically (a layered earth), and to have band-limited, periodic horizontal variation. The discretisation within any one layer will be characterised by M points in the horizontal direction(s) with spacing equal to the sample spacing. If there are N layers in the vertical direction (with some problem-dependant spacing) then there are MN source degrees of freedom.

By applying Equation (3.1) to each horizontal layer separately, we could obtain N different source layers at different depths, each of which will generate the measured response f. This is just the well known idea that any data can be attributed to an equivalent layer source. Explicitly, let $\hat{f}(\mathbf{k})$ be the $\mathbf{k}^{th}$ Fourier coefficient of $\hat{f}$ in a discrete Fourier transform (DFT) of the regularly spaced measurement f. (That is, $\mathbf{k}$ is now a vector of integers). Also, let $\hat{g}_i(\mathbf{k})$ be the $\mathbf{k}^{th}$ discrete Fourier coefficient of the ith layer influence function (Equation (2.10) or (2.19)). Suppose for the moment that $\hat{g}_i(\mathbf{k}) \neq 0$ for all i and $\mathbf{k}$. Then an equivalent layer source in the position of the ith layer of the source domain is given by

$$\hat{S}_i^{eq}(\mathbf{k}) = \hat{f}(\mathbf{k}) / \hat{g}_i(\mathbf{k}) . \tag{3.2}$$

It follows that $\hat{S}_i^{eq}(\mathbf{k}) = 0$ for all i (and given $\mathbf{k}$) if and only if $\hat{f}(\mathbf{k}) = 0$. Let us now consider a new source distribution constructed from these particular equivalent layer solutions, viz.

$$\hat{S}_i(\mathbf{k}) = w_{\mathbf{k}i}\hat{S}_i^{eq}(\mathbf{k}) \qquad i = 1, N \tag{3.3}$$

where now $\hat{S}_i(\mathbf{k})$ is the $\mathbf{k}^{th}$ Fourier coefficient of the new ith source layer. Suppose further that

$$\sum_{i=1}^{N} w_{\mathbf{k}i} = 1, \tag{3.4}$$

for each individual $\mathbf{k}$. The superposition of the new source layers $\hat{S}_i$ then generates f as follows;

$$\sum_{i=1}^{N}\hat{S}_i(\mathbf{k})\hat{g}_i(\mathbf{k}) = \sum_{i=1}^{N}w_{\mathbf{k}i}\hat{S}_i^{eq}(\mathbf{k})\hat{g}_i(\mathbf{k})$$
$$= \sum_{i=1}^{N}w_{\mathbf{k}i}\hat{f}(\mathbf{k}) \qquad . \tag{3.5}$$
$$= \hat{f}(\mathbf{k})$$

Thus, the collection of layers described by $\left\{\hat{S}_i\right\}_{i=1,N}$ constitutes a possible source distribution in the domain $z < 0$ that exactly matches the measured data f.

Conversely, consider any compatible source distribution $\hat{S}_i(\mathbf{k})$ such that

$$\sum_{i=1}^{N}\hat{S}_i(\mathbf{k})\hat{g}_i(\mathbf{k}) = \hat{f}(\mathbf{k}) \tag{3.6}$$

and suppose for the moment that $\hat{f}(\mathbf{k}) \neq 0$ for all $\mathbf{k}$. Then we may define some new

$$w'_{\mathbf{k}i} = \hat{S}_i(\mathbf{k})/\hat{S}_i^{eq}(\mathbf{k}) \tag{3.7}$$

since $\hat{S}_i^{eq}(\mathbf{k}) \neq 0$ for all i, $\mathbf{k}$. Consequently,

$$\hat{f}(\mathbf{k}) = \sum \hat{S}_i(\mathbf{k})\hat{g}_i(\mathbf{k})$$

$$= \sum_{i=1}^{N} w'_{ki}\hat{S}_i^{eq}(\mathbf{k})\hat{g}_i(\mathbf{k}) \quad , \tag{3.8}$$

$$= \sum_{i=1}^{N} w'_{ki}\hat{f}(\mathbf{k})$$

which implies that $\sum_{i=1}^{N} w'_{ki} = 1$ for all $\mathbf{k}$ such that $\hat{f}(\mathbf{k}) \neq 0$. Thus, under the stated condition on $\hat{f}$, any compatible $\hat{S}_i(\mathbf{k})$ can be expressed in the form (3.3) with weights satisfying (3.4).

Now consider $\hat{f}(\mathbf{k}) = 0$ for some given $\mathbf{k}$. In this case, the condition on the $\hat{S}_i(\mathbf{k})$ becomes

$$\sum_{i=1}^{N} \hat{S}_i(\mathbf{k})\hat{g}_i(\mathbf{k}) = 0 \tag{3.9}$$

for all $\mathbf{k}$ such that $\hat{f}(\mathbf{k}) = 0$. Whenever we find this situation arising in practice (i.e. $\hat{f}(\mathbf{k}) = 0$ for some $\mathbf{k}$) then we replace Equation (3.3) with

$$\hat{S}_i(\mathbf{k}) = w_{ki}/\hat{g}_i(\mathbf{k}) \tag{3.10}$$

(absorbing the change in physical units into these specific w_{ki}) and also replace the corresponding Equation in (3.4) with

$$\sum_{i=1}^{N} w_{ki} = 0 \tag{3.11}$$

for each $\mathbf{k}$ such that $\hat{f}(\mathbf{k}) = 0$. With this minor modification, we have the characterisation of the entire ambiguity domain at a given resolution whenever $\hat{g}_i(\mathbf{k}) \neq 0$ for all i and $\mathbf{k}$. We note that the null space of the problem (set of annihilators) could be characterised in terms of (3.10) and (3.11). By linearity, we could then span the ambiguity domain by adding any $\hat{S}_i^{eq}$ (or any other particular solution) to this null space. Instead we choose the characterisation (3.3) and (3.4) and resort to (3.10) and (3.11) only for $\mathbf{k}$ such that $\hat{f}(\mathbf{k}) = 0$.

There are a few reasons for this choice. Firstly, it is quite rare in practice for $\hat{f}(\mathbf{k}) = 0$, and so (3.10) and (3.11) are rarely needed. More important, the equivalent layers $\hat{S}_i^{eq}$ are a natural set of particular solutions to the inverse

problem. Consequently, Equation (3.3) has an intuitive meaning as a weighted combination of components of these natural solutions. This particular linear combination also bestows greater importance upon positive w_{ki} than would be the case if the classical null space characterisation were used. Algorithmically, this makes it easier to control the sign (and more generally the range) of $S_i(\mathbf{x})$.

The remaining problem is when $\hat{g}_i(\mathbf{k}) = 0$. From Equation (2.10) we see that this does not occur in the gravity case, but can occur in the magneto-static case (2.19) when $\mathbf{k=0}$ or when the ambient field and the magnetisation are orthogonal under $\vec{\Lambda}$. This leads to a further source of ambiguity in the magneto-static case, over and above that discussed so far. For example, the case when $\mathbf{k=0}$ is the well known phenomenon that an infinite layer with constant magnetisation produces no measurable field away from the layer (since the dipole contributions at every point off the layer cancel). In most of the following, we will be considering the gravitational field, which is free of these particular ambiguities.

4 The Extent of Ambiguity in Potential Fields

In this section, several simple anomalies are analysed. Using the constraint Equations (3.4), the entire ambiguity domain for these anomalies could (in principle) be reconstructed. We demonstrate that, even in simple cases, the ambiguity domain is huge.

4.1 The Limitation of Using Simple Geometry

Figure 4.1 presents a gravity profile. Commonly, two basic assumptions would be employed in inverting such a profile. Firstly, a regular, well defined, single anomalous body is assumed to be present. Secondly, the location of the body is assumed to be underneath the positive anomaly in the profile.
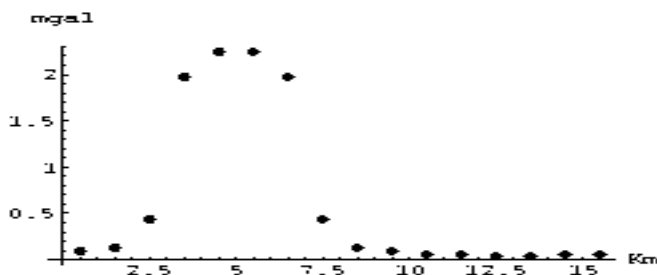
Figure 4.1 Gravity profile obtained by forward modelling the density contrast distribution presented in Figure 4.2.

11

The actual source distribution used to generate Figure 4.1 is presented in Figure 4.2. It represents the 2-D section of a rectangular prism with density contrast 0.2 g/cm^3, infinitely extended perpendicular to the section. Such a model would satisfy both of the assumptions of the previous paragraph.

Figure 4.2 2-D vertical section of a prism infinitely extended perpendicular to the section, whose density contrast with the surrounding material is 0.2 g/cm^3. This model has been used to obtain the synthetic profile presented in Figure 4.1. Here, as in all of the 2-D plots presented in this section, black corresponds to a density contrast of -0.2 g/cm^3, while white corresponds to 0.4 g/cm^3 density contrast.

Figure 4.3 displays four models obtained by inverting the profile in Figure 4.1 using the procedure described in the previous section. Each is due to a different set of parameters w_{ki} in Equations (3.4). They all yield accelerations that match the profile in Figure 4.1 exactly.

(a)　　　　　(b)

(c)　　　　　(d)
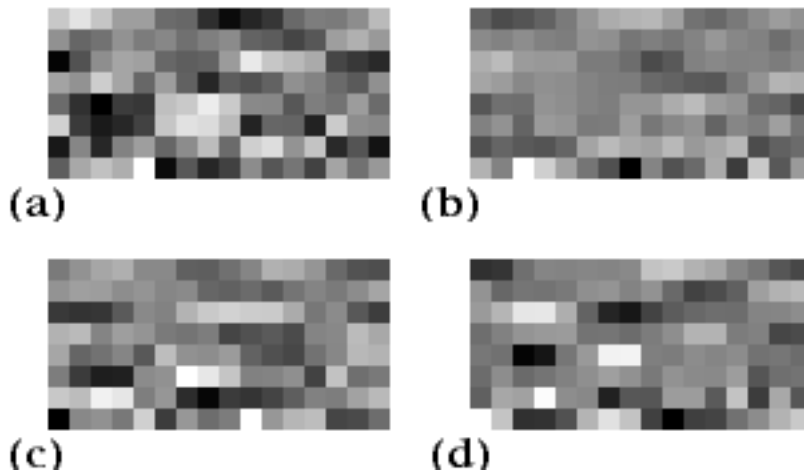
Figure 4.3. Four examples from the ambiguity domain associated with the profile of Figure 4.1. Density distributions vary drastically from the model presented in Figure 4.2. No clear isolated body can be seen, nor any clear increase in the density contrast in the area immediately underneath the positive peak in the profile in Figure 4.1.

Two related points are clear. Firstly, no regularly shaped, anomalous bodies are necessary to interpret the profile under analysis. Secondly, a very

irregular, scattered distribution of material could be responsible for the same profile. *An infinite number of models similar to the ones in Figure 4.3 could be generated with the same technique.* Later in the paper, we discuss the physical/geological feasibility of these models. For the moment, notice that they all have geologically feasible density contrasts.

From this example, we conclude that limiting the possible outcomes of an inverse calculation to bodies characterised by simple geometry implicitly disregards a huge number of possible models. In the example above, no scattered distribution of small anomalous bodies would be allowed if the search was limited to a single, regularly shaped anomalous body. Consequently, simple geometry constitutes a very strong assumption on the inversion that should only be imposed when justified by reliable *a priori* geological information.

4.2   Forcing the Location of Anomalous Bodies

Another common practice in the inversion of potential field data is to locate causative bodies underneath the main anomalies in the profile. This spatial relationship is also at the heart of the visual interpretation of potential field maps. Here we want to check the validity of this assumption.

Figure 4.4 shows two more exact inversions of the profile in Figure 4.1. In these examples the positive anomaly in the profile is due to a scatter of relatively dense material, while a larger anomalous body is located in a different horizontal position, (just underneath the flat part of the profile). Its effect is compensated by the distribution of less dense material surrounding it, and its presence is apparently concealed in the data. Although without specific *a priori* information it would be impossible to reconstruct the presence of the body from the data, this example shows that the location of large anomalous bodies underneath the major anomalies should not be taken for granted. Large anomalous bodies may be located underneath featureless parts of the potential field data, depending upon the distribution of the surrounding material.

(a)   (b)
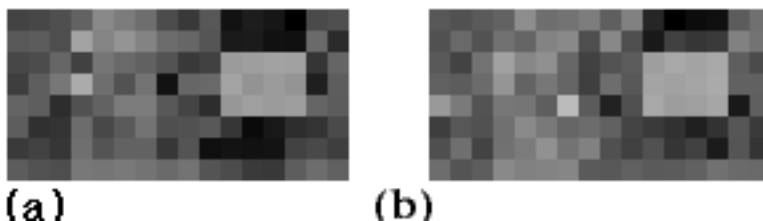
Figure 4.4. Two models satisfying the gravity profile in Figure 4.1. As can be seen, the horizontal position of the large anomalous body does not coincide with the positive peak in the profile. Its presence is compensated by less dense material surrounding it and is concealed in the profile.

4.3   Depth Ambiguity

The most serious and best known source of ambiguity is the depth of causative bodies. This is demonstrated by Figure 4.5, in which possible solutions characterised by bodies at different depths are presented. They all generate the profile in Figure 4.1 exactly.
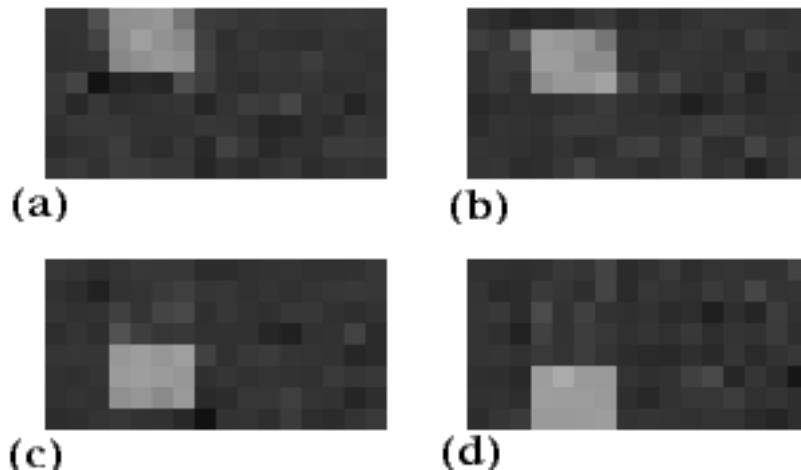
Figure 4.5. Four more models satisfying the gravity profile in Figure 4.1. They all resemble very closely the model in Figure 4.2, however, small variations in the density contrast at each node allow for the anomalous body to change its vertical position considerably. Such position cannot be recovered solely from the gravity profile, since each model reproduces the data exactly.

An analogous example is given in Figure 4.6. Figure 4.6a shows a synthetic model used to generate a gravity profile. It simulates the presence of an irregular basement. Figure 4.6b, c and d show three models, generating the same gravity profile, each having the basement at a different depth. Obviously, the depth to the basement can not be recovered by simple analysis of the potential field data. We therefore caution about the rote application of methods such as Werner deconvolution (Werner 1953; Naudy 1971) or the spectral methods from Spector and Grant (1970). The pertinent questions to be asked of such methods are "What are the (perhaps implicit) *a priori* constraints being imposed by the method?" and "Are the constraints justified in the region under study?".
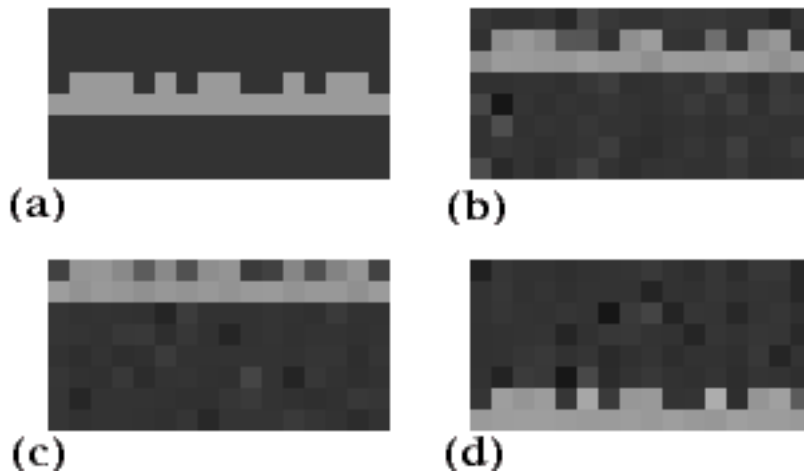
Figure 4.6. Synthetic model used to generate a synthetic gravity profile (a) simulating the presence of an irregular basement. Panels b, c and d show 3 models, satisfying the same gravity profile, each characterised by the basement at very different depth.

5 The Mickey Mouse Effect

From the previous experiments it is obvious that completely different geological models could fit the same potential field data. In this section we want to be even more pessimistic and state that almost **any** idea on the nature of the solution, even the most bizarre, could still be slightly modified to fit the data under analysis. A few synthetic examples will illustrate this statement.

Suppose that a fictional explorer is convinced that an ore body with the shape of Mickey Mouse™ is the target of an exploration survey. Figure 5.1 shows an example of such an ore body. A gravity survey is conducted over the area and the resulting profile is inverted in order to find a model that simultaneously fits the data, and resembles the Mickey Mouse ore body. One might suppose that if a model resembling Mickey Mouse can be found that fits the data reasonably well, then the existence of such a curious ore body is confirmed. Unfortunately this supposition would be false.

In the top row of Figure 5.2 a number of models are shown. They represent simplified sketches of possible geological configurations, resembling, respectively, a dipping fault, a folded layer and an isolated body (the same model studied in the previous sections). The second row shows the gravity profile obtained from forward modelling these sources. For each profile an inversion has been performed in which we search for a model that resembles the Mickey Mouse ore body in Figure 5.1 as closely as possible. The results are shown in the bottom row. For each profile a Mickey Mouse ore body, *in exactly the same location*, can be found that *exactly* fits the data. Once again, the density contrasts are all in geologically realistic ranges.
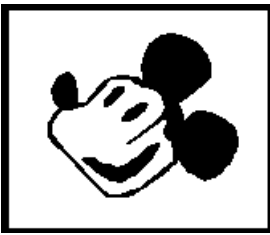
 Figure 5.1. A 'cartoon' section of the Mickey Mouse ore body (hand sketched by the authors). It will be discretized to a 32*32 pixel source distribution for the inversions.
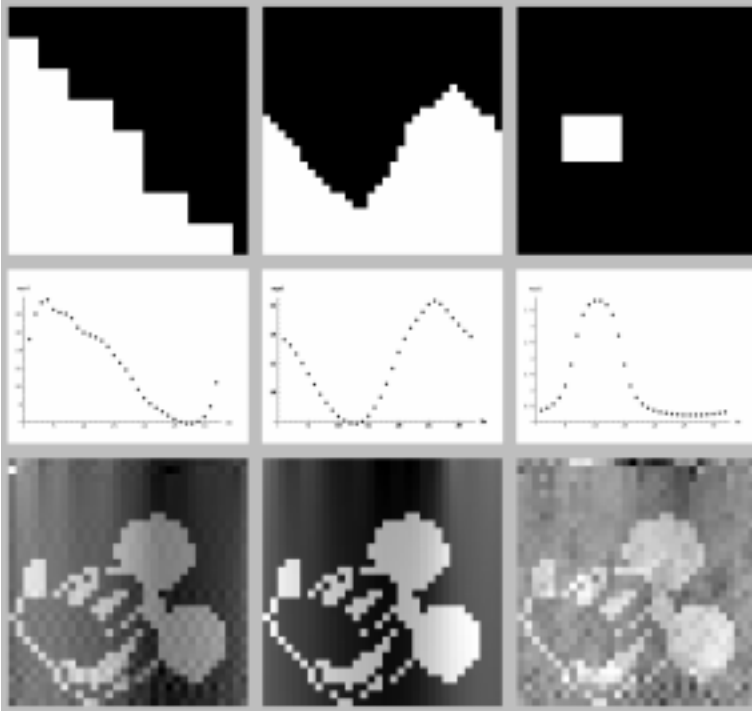
Figure 5.2. In this experiment we show that even the most bizarre geological interpretations could still fit potential field data under analysis. The top row shows three models while the second row depicts the corresponding gravity profiles. For each of these profiles a Mickey Mouse ore body, in exactly the same location, can be found that exactly matches the data.

We can be even more general and state that for *any* profile we will be able to find a Mickey Mouse ore body able to fit the data. The generality of this statement is guaranteed by an image like the one in Figure 5.3. It represents a Mickey Mouse image that gives zero field, i.e. a completely flat profile of zero gravity anomaly. This is an example of an annihilator.

Figure 5.3. This Mickey Mouse image has the property that it has a 0 gravity field when used in a forward calculation. It is a homogeneous solution belonging to the null space of 2-D inverse gravity problems. Such a source distribution can be added to the solutions of any inverse problem (with the same horizontal resolution) and still give a source that fits the data exactly.

5.1   Comments

It is clear now that potential field data alone are not a sufficient constraint for an inverse problem. Without *a priori* information, **potential field data are not adequate to confirm a geological model**. If an inversion is constrained towards a particular model, without justification by accurate *a priori* information, the result may lead to erroneous geological interpretations. The only rigorous possibility is the use of the potential field data to refute a given hypothetical interpretation. However, we have also seen that the ability of such data to refute hypotheses is limited, as evidenced by the Mickey Mouse effect.

We can easily quantify the dimensionality of the ambiguity domain. If one inverts for the $M \times N$ source model discussed above, each of the M wave-vectors has N degrees of freedom. Equivalently, any solution can be represented as a single point in an MN dimensional parameter space of the w_{ki}. Geometrically, the constraint Equations (3.4) can be viewed as the equations of M different hyperplanes, each of dimension (MN-1). That is, each constraint reduces the available number of degrees of freedom by one. The aggregate space is the intersection of the individual hyperplanes, which are clearly linearly independent. Thus, any model that exactly matches the observations still has $M(N-1)$ freedoms, and this is the dimension of the ambiguity domain (the size of the space of annihilators, or the nullity of the problem).

The classical characterisation of the possible solutions to this problem is as the null space translated by a particular solution. (That is, the particular solution plus some homogeneous parts.) Our characterisation differs slightly from this, since it corresponds to a (component-wise) convex sum of particular solutions, Equations (3.3).

17

Essentially the same analysis applies to the potential energy $V(x, y, z)$ (using appropriate layer source influence functions), so that it is no use appealing to the vector fields ($\vec{B} = -\nabla V$ or $\vec{g} = -\nabla V$) to overcome the ambiguity problem, nor to any other quantity derivable from the potential energy. Further, the recovery of an arbitrary magnetisation vector field $\vec{m}(\vec{x})$ would require even more *a priori* information.

Clearly, some of the model sources presented above are not geologically realistic. However, they all incorporate aspects of reality. The density and/or susceptibly contrasts employed are within a feasible range, and the level of complexity in the solutions is more realistic than simple geometric shapes. The next section focuses on selecting solutions with geologically feasible constraints.

Note, that the concept of 'geologically feasible' is still not well defined from a mathematical, physical, statistical, or even geological point of view. A few previous attempts at a definition have been made (Pilkington, Gregotski and Todoeschuck (1994), Pilkington and Todoeschuck (1990)). Such attempts could be incorporated into the procedure described in this paper. In addition, our procedure could be extended to include any future criteria.

6   Selecting Appropriate Solutions

Based on *a priori* information about the area under analysis, let us now seek to restrict the number of possible solutions. The simplest expression of the ambiguity domain is in Fourier space. The parameters w_{ki} are just weights of the Fourier source spectra for each equivalent layer participating in the solution. Unfortunately, interpreting the w_{ki} directly in terms of physical or geological constraints is not simple. In this respect, the parameterisation is not much better than Mareschal's Laguerre coefficients (1985). Because of this, restrictions due to *a priori* information must be indirectly applied to the parameters w_{ki} (e.g., through iterative search).

The search we advocate here is fundamentally different from traditional iterative inversions. In traditional search methods, one searches the entire domain (defined by the problem parameterisation) for models that satisfy the data (plus, in some cases, further *a priori* information). This results in a model, or a limited number of models, fitting both the data and the additional constraints to within some specific tolerance.

In the method proposed in this paper, we search only inside the ambiguity domain (i.e., only among models that fit the data exactly). Consequently any end result from the inversion will exactly satisfy the potential field data at the full resolution of analysis. Among these models, we search for models that also satisfy other requirements.

Contrast our approach with the traditional approach of simplifying the problem by using bodies characterised by simple geometry. Two major differences are found. Firstly, we ask for solutions to resemble statistics of the data under analysis, while other techniques force solutions into a particular shape by limiting the search domain. Secondly, our method allows for different kinds of geological structures to be modelled (faults, folds, isolated bodies, layers etc..) depending on *a priori* information, while most traditional methods allow for only one kind of structure depending of the parameterisation adopted.

6.1   The use of *a priori* information

One of the aims of the inversion scheme presented here is to use as many kinds of geological and physical *a priori* constraints as possible. The different kinds of *a priori* constraints commonly available can be broadly divided into two classes:

1) Accurate 'ground truth' information. This may include density or susceptibility measurements from drilling, or geological cross sections considered particularly reliable, or perhaps surface geology. This kind of information will be called 'hard' information in the rest of the paper.

2) General information on the geological style of the area. This may come from large scale studies on the area, or from small scale, detailed studies on adjacent areas that are considered to be somehow related to the area under analysis. Such information might be summarised in a geological cartoon representing the style of the area, or it might be a high-resolution sampling of some quantity from a similar region, or it might even be as detailed as a geostatistical variogram (or other statistics) for the region. This kind of information will be referred to as statistical or 'soft' information in the rest of this work.

A necessary condition for soft information to be useful in a search is that it is quantifiable. For an example drawn from geostatistics (Journel, personal communication, 1995), a geological cartoon might be translated into a variogram via level curves of some relevant quantity (e.g. isopachs) or directly turned into a suite of indicator variograms. Clearly, the short-range parts of such variograms are poorly constrained. However, the long range parts quantify aspects of the interpreter's geological knowledge of the area, and might be useful to provide quantitative constraints on long-range correlations. Inversion techniques could then be used to find solutions that match all such information simultaneously. Of course, the advantage of autocorrelation information is that it can be calculated from the Fourier representation of a trial source distribution. This eliminates any need for back transformation of a trial solution to the spatial domain during the search.

6.1.1 Statistical (soft) information

To date, we have tried our technique using two different statistics, autocorrelation (to represent long range behaviours with two-point statistics), and a local multi-point statistic (designed to represent short-range textures).

The local multi-point statistic comes from scanning a template over some prototypical model. At each position, the template lies over (say) $m \times n$ pixels.   We construct a corresponding mn dimensional 'state space' by plotting the value in each pixel along a coordinate axis. Thus, each template position defines a point in the state space. When the entire prototype model is scanned, a set of state space points is obtained, the configuration and density of which contains information about local textures. Note that this method is a higher dimensional probabilistic extension of the idea underlying recent nonlinear analyses of time series (e.g. Packard et al., 1980). The method also represents essentially the same statistic as captured by the 'schéma glissant' of Matheron (1978) (for an English language description see also, e.g., Journel, 1997). Autocorrelations are calculated from prototype models in the standard manner (e.g. Press et al., 1992 p545; Isaaks & Srivastava 1989).

In the examples shown in this paper, the synthetics used for our forward models are also used to calculate our statistics. In this sense, our statistical information is the best possible. In practice, prototypes might come from exhaustive sampling of some (small) region of similar geology, or they might come from adjacent regions.

During the search of the ambiguity domain, a comparison is performed by calculating a misfit measure between the prototype model and the current candidate inversion. In the case of autocorrelation, the misfit will be just the squared difference between the autocorrelation of the prototype model and that of the candidate inversion. For the local multi-point statistic, we define the misfit as the average of the minimum distances between the state space points obtained from the prototype and those points generated by a candidate inversion. We acknowledge that such a definition of misfit imposes a metric upon the state space that may or may not be valid for the process(es) under study. However, we suggest that the technique's success in this study is evidence that such a metric is useful. We have also tried a linear combination of these two misfit criteria.

In all cases we attempt to find solutions that minimise the misfit. It is clear that the problems are non-linear in nature, containing multiple local minima. An attempt to use a simple local search (the SIMPLEX method from Press *et al.* (1992)) yielded very poor results. Better results are obtained from the use of a global search performed with a Genetic Algorithm (GA). A description of the Genetic Algorithm used in this research can be found in Boschetti, Dentith &

List (1996). The particular characterisation of the search space in terms of the w_{ki} fits nicely into a GA encoding.

Figure 6.1 displays the style of results that may be obtained with this approach. Four synthetic models used to generate the data set are shown in the top row. The four models represent respectively (a) an isolated anomalous body (similar to the gravity cases already presented), (b) a dipping fault, (c) a deep basement overlaid by less dense material and (d) a combination of the anomalous body in (a) and a shallow dyke. These models are all characterised by 16 blocks in the horizontal direction and 8 blocks in the vertical direction, resulting in a 128 dimensional space for the GA to search.

The second row represent the results of the inversion when autocorrelation has been used as the misfit criterion. In all cases the actual synthetic model has been used as a prototype.

It can be seen from the images in the second row that the use of autocorrelation as a misfit criterion helps in recovering images characterised by a style and a texture close to that of the prototypical model, when compared to inversions based solely on matching the potential field. This is particularly clear for the model in column (a) and (d). The example of the rectangular anomaly in column (a) should be compared to Figure 4.3 (the inversion of the gravity profile in Figure 4.1 without *a priori* statistical information). It is clear that in this case the algorithm 'knows' it has to look for a single anomaly with an appropriate shape, surrounded by a mostly constant background. The extent of scattered material in the domain is now relatively limited.

Note that the use of statistical information is not enough to make the problem unique. Solutions from different runs differ (much as they do in geostatistical conditional simulation techniques). However, the appearance of the solution is always very close to the prototype model. Large variation can be found in the vertical position of the causative body. This result is in line with the inversion shown in Figure 4.5.

Better results are obtained with the use of multi-point statistics as can be seen from the images in row 3. Now the texture and style resemblance is even stronger. However, in both cases the existence of the ambiguity domain is still clear, especially in the inability to exactly fix the vertical position of the causative bodies. The fourth row in the figure shows the inversion simultaneously using autocorrelation and multi-point statistics as the misfit criteria. Clearly only marginal improvement is obtained.

The weakness uncovered by these results is not entirely surprising, since the statistics are translation invariant measures of source variation. Consequently such *a priori* information could not be expected to help much in determining

source position. Such measures are, however, helpful in determining things such as lumpiness and texture.
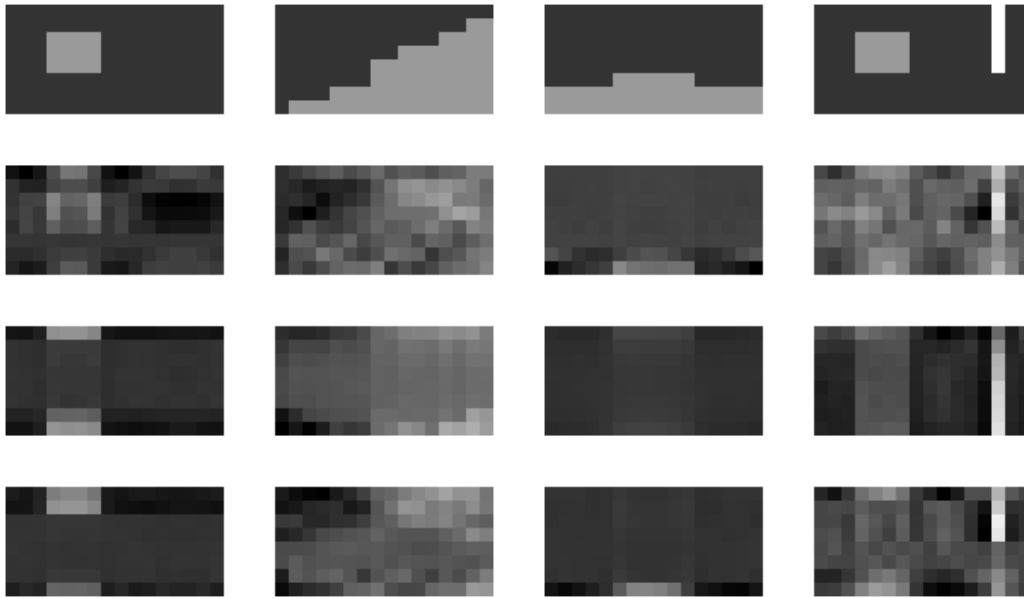
Figure 6.1. 2-D test of the inversion of magnetic data with statistical *a priori* information. In the top row we depict the four synthetic models used to generate the potential field anomalies. In the second row we present examples of the inversion using the autocorrelation of the prototype model as *a priori* information. (In all cases the synthetic has been used as prototype model). The third row shows examples from the inversion using multi-point statistics as the search criterion. The last row presents the results when both autocorrelation and multi-point statistics are combined to form a search criteria.

6.1.2 Hard information

We have seen how prototype models of the area under analysis can be used to reconstruct solutions that resemble particular geological styles. When ground information is available (and considered particularly reliable) it can be used to constrain the problem more strongly. This can be achieved by asking the solution to respect *a priori* density/susceptibility values at some nodes. Two situations might typically occur.

Firstly, through some integrated geological/geophysical surveys we might possess a geological section considered particularly reliable and we may want to slightly improve the section by asking it to satisfy the potential field data. This is equivalent to searching the ambiguity domain for the solution that is closest to the input geological section, where the closeness can be measured in a least squares sense. Notice the difference between this approach and the one described in the previous section. Asking a solution to statistically resemble a

prototype model means asking for the solution to have the same texture, or to possess similar features but possibly at different locations. Now we ask the density/susceptibility values to be approached pixel by pixel (as in the Mickey Mouse example, with all of the attendant dangers).

Secondly, some downhole information may be available from the area under analysis. This is basically similar to the previous case with the difference that constraints are limited to only some nodes. Where samples do exist, they truly constitute 'hard' information, and not the 'softer' information of the inferred cross-section of the foregoing.   When there are only a few nodes, the ambiguity domain is reduced but remains very large. However, this kind of information is very useful when used in conjunction with statistical information. Previously, we saw that solutions obtained by matching the autocorrelation or the multi-point statistics with a prototype model have a general appearance similar to the input model, but it is not possible to fix the vertical position of the causative bodies. The use of underground information greatly helps in this task. We also note that, given statistical information and the potential field, it is almost as useful to know where the anomaly is *not* as it is to know where it is. Thus, 'dry well' hard data is still useful in tying down a solution.

In Figure 6.2 we see the results from inverting the same data sets as in Figure 6.1 when the information from two drillholes is used. The two drillholes provide the density contrast, and are assumed to be deep enough to reach the bottom of the domain. They are located at columns 4 and 13 in the model (recall that the model consists of 8*16 pixels). It is clear that, especially for the examples a, c and d, that the presence of the underground information is enough to allow the detection of the approximate vertical location of the anomalous body. The dipping fault example, panel b, is much harder and the solution less satisfactory. However, even in this case an improvement over the inversion with only statistical information is apparent.

(a)

(b)

(c)

(d)
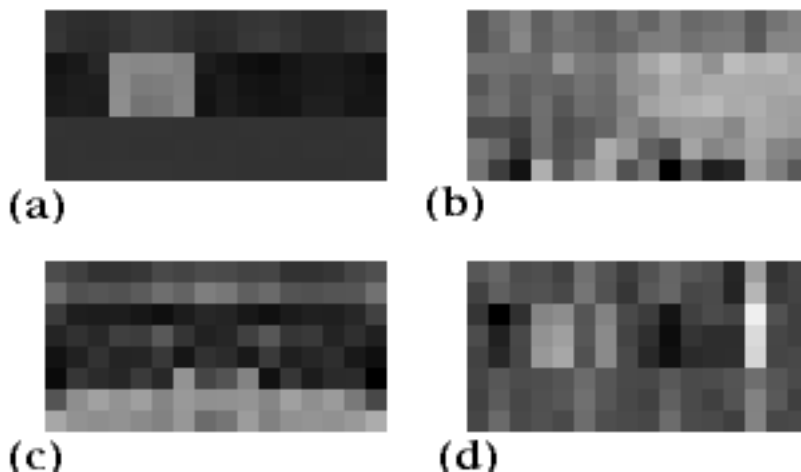
Figure 6.2. Result from the four models presented in Figure 6.1 when underground information has been used in the form of two drill-holes.

7   Extension To 3-D

We saw that the construction of the ambiguity domain does not involve any iterative search and that, due mainly to the Fourier domain implementation, it is actually computationally very cheap. The extension to the 3-D case is not a major concern from this point of view. However, the inversion to find models that satisfy the *a priori* data does involve iterative search and the increase in the computational time required by this operation when applied to a 3-D case is substantial. A considerable increase in the dimensionality of the problem in 3-D is the cause of this increased demand. A model of 16*16*8 blocks represents a 2048 dimensional space. Global search methods, such as GAs, are usually applied to much smaller dimensional problems, rarely exceeding a few tens of unknowns. Although Boschetti et al. (1996) and Mathias et al. (1994) showed that larger dimensional spaces may be tackled by the use of modified GAs, one must expect GAs' performance to be almost at a limit in this application, and, at the very least, to expect quite a long convergence time.

Accordingly, we kept the dimensionality of the problem relatively low. In the example shown below, the 'realistic synthetic' case is characterised by 16*8*8 blocks, while the real test has been performed on a 16*16*4 model, both resulting in 2048 dimensions. Although this dimensionality may appear small for exploration applications, it should be noted that it greatly exceeds the typical dimensionality of standard inversions of potential fields found in the literature.

7.1   A Realistic Synthetic Example

A data set of ore grades sampled in a gold mine in Western Australia has been nonlinearly transformed into density contrasts. The resulting model was then used to generate a 2-D gravity data set. The model data were also used to calculate the target autocorrelation.

Two inversions were performed. In the first inversion only statistical data have been used, i.e., the search for suitable models has been performed simply by matching the autocorrelation of the prototype model with the candidate inversion. A few test runs showed that the appearance of the solutions obtained in this way resembled the prototype model but they still showed a quite large variability.   This is in accordance with the results presented for the 2-D case.

In the second inversion both statistical data and hard information (in the form of four drillholes randomly placed in the domain) have been used. The four

drillholes are assumed to reach the bottom of the domain. This is equivalent to constraining the density values along four columns in the model. In this instance a few test inversions showed that the results tend to be very similar, i.e., the problem is much better constrained with the use of underground information and the ambiguity domain is greatly reduced. An example from the inversion is presented in Figure 7.1. On the top, the synthetic density model is shown; on the bottom left, the result from the inversion using both statistical and direct data in form of drillholes; on the bottom right, the result using only autocorrelation data. Both solutions resemble the original data set, however the improvement seen in the bottom left result clearly shows the value of (even limited) hard data.
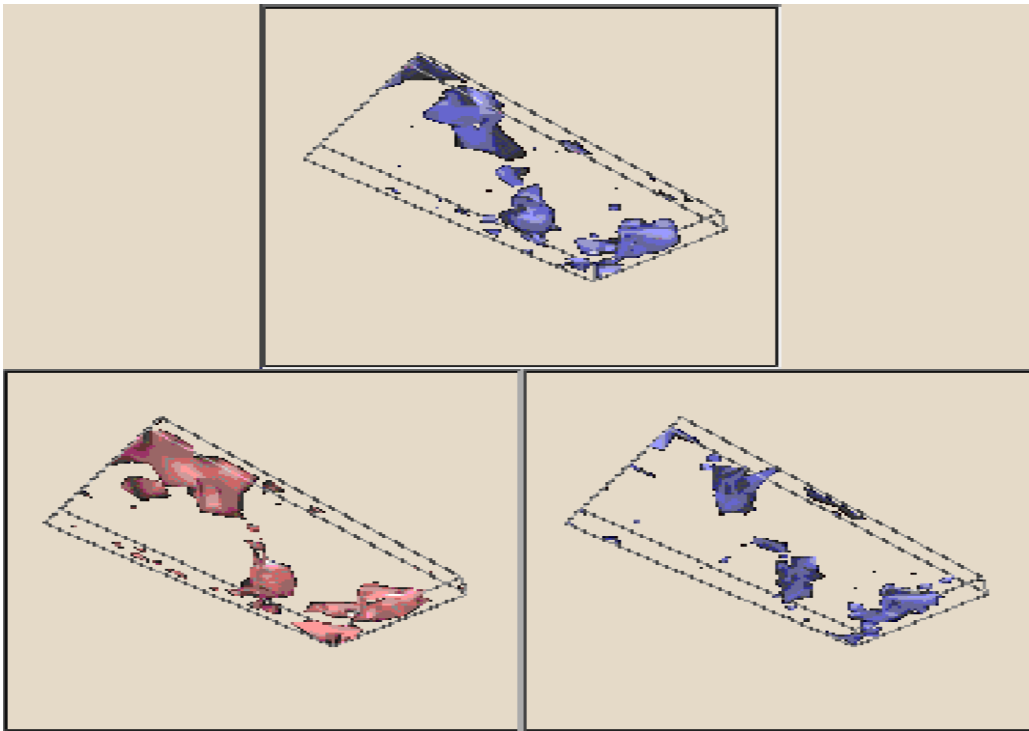
Figure 7.1. Example of inversion of potential field data in 3-D. The top figure shows the synthetic model used to generate a gravity data set. It consists of real ore-grade values artificially transformed into density contrasts. On the bottom left is the result from the inversion when both statistical and direct data in form of drillcore intersections are used. On the bottom right an instance from the set of solutions obtained when only statistical data are used.

7.2   Inversion with Limited Real Data

The method has also been tested on a real total field magnetic data set collected for experimental purposes by Western Mining Corporation in Western Australia. In order to obtain a gridded data set the flight line measurements (sampled at 25 metres from the surface) have been interpolated into a 16*16 node grid, with 25 metre spacing in both the horizontal directions. These are also the horizontal dimensions of the calculation domain, while in

the vertical direction four layers, 25 metres thick, have been modelled. In order to remove the regional trend, the gridded data set has been fitted to a plane and the residual has been used in the inversion. This also justifies the limited depth extent of the calculation domain.

A number of downhole samples (along two parallel lines, cutting through the calculation domain) were available, with measurements of susceptibility along the cores. These values have been used in two ways. The actual values at the drillhole location have been used as hard information in the inversions, i.e., the target solution has been asked to satisfy these values at the corresponding blocks. Also these values have been interpolated on the entire domain and the result has been used as a statistical model. Basically in this way we ask for a smooth solution. This is rationalised by the fact that no other information was available on the area.

The result of the inversion can be seen in Figure 7.2. On the left-hand side we have the interpolated values and on the right-hand side the result from the inversion. This corresponds to a modification on the original image in order to satisfy the potential field data and the required constraints. A more sophisticated approach could be attempted where more underground information, or better statistical information, is available.
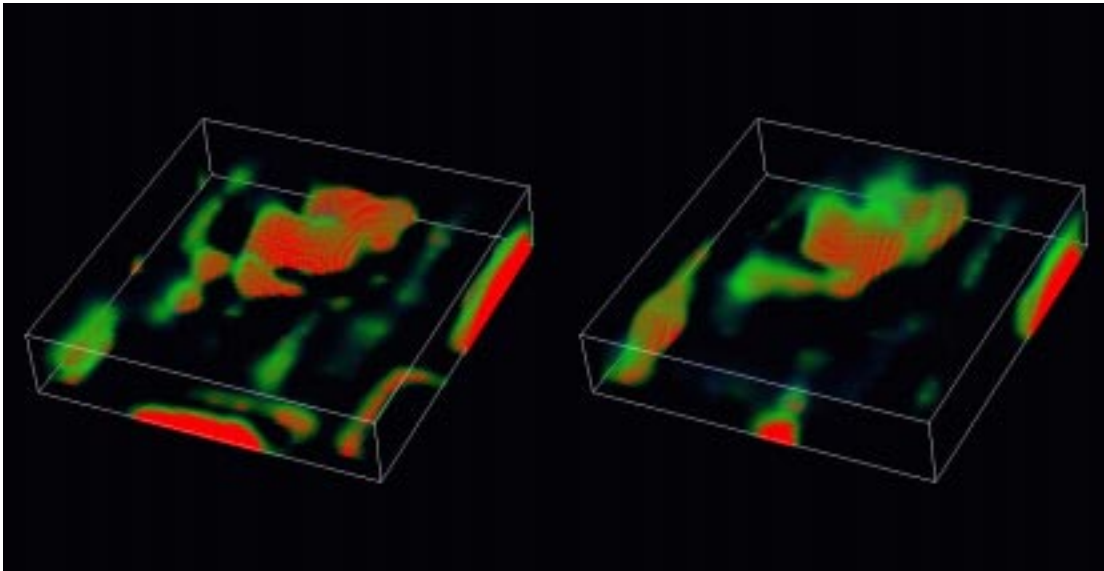
Figure 7.2. Image used as a statistical model in the 3-D inversion of the real data set (left-hand side) and the result from the inversion (right-hand side). The solution satisfies the magnetic data set and closely resemble the statistical model.

8   Conclusions

The entire ambiguity domain (at a given resolution) can be expressed as a particular mixed superposition of equivalent layer sources. Within the potential field measurements in free space, there is at most enough information to define the equivalent of one source layer. The resulting ambiguity allows models of almost any visual appearance to fit the potential field data exactly. Even completely wrong geological interpretations could be slightly modified in order to fit a particular anomaly, and consequently the result from the inversion of potential field data without further constraints should be considered, at the very least, inconclusive.

Conversely, this work also suggests caution in the use of inverse methods that impose strong assumptions directly in the problem parameterisation, since entire families of possible solutions might be discarded spuriously. At the very least, such techniques as Werner and Euler deconvolution and 'model free' inversions involving smoothness assumptions should only be applied with a clear understanding that it is these assumptions that are determining the solution, more so than the data.

Seeking models within the ambiguity domain whose spatial variation is statistically similar to some prototypical model(s), leads to solutions that display similar textural character to the prototypes. However, since the statistical measures we have used are translationally invariant, there is still a large amount of translational freedom in the solutions, especially vertically.

Once the textural character has been constrained by the *a priori* data, and some of the horizontal variation pinned down by the potential field constraint, hard data, even 'dry well' data which does not intersect anomalous bodies, is most effective in improving the results.

The ambiguity domain is best expressed in the 2-D Fourier domain, where the 'constraints' provided by the potential field are diagonal in **k**, and of (matrix) bandwidth N in z. The autocorrelation of a given source distribution is also easily expressed in the Fourier domain. There are also indications that some local multi-point statistics can be given a simple Fourier characterisation, along the lines of Wiener prediction theory. Thus, our statistical information, like any other translation invariant measure, can be expressed in a natural way in the Fourier domain.

As long as such statistics are easily expressed in the Fourier domain, the search over the ambiguity domain can be confined entirely to the Fourier representation. If the misfit criteria are sufficiently simple, then the statistical *a priori* requirements could be expressed as linear constraints on the w_{ki}. Moreover, suitable choice of statistics could lead to banded equations, potentially eliminating the need for a search entirely.

On the other hand, hard data is best expressed as constraints on the values of the source at specific locations in the spatial domain. If expressed as

constraints (rather than as a minimisation), these equations, while diagonal in the spatial domain, are full in the Fourier representation.

This is the usual problem that arises in data fusion, in this case related to the complementary nature of dispersion in the spatial and Fourier domain. One representation makes one set of constraints appear simple, but causes another set to become complicated. Clearly, one would like to find a compromise domain in which all the constraints are banded (in the matrix equation sense). To this end, we have begun investigation into wavelet bases (Hornby *et al.*, 1998) and piecewise constant source distributions. This work naturally leads to more general considerations of precisely when a unique or low variability solution can be expected to exist, and what the minimal, and (from a geological standpoint) most widely applicable *a priori* assumption might be that leads to this situation. We believe this calls for a delicate balance between mathematical parsimony and geological common sense.

Acknowledgements

REFERENCES

Al-Chalabi, M., 1971. Some studies relating to nonuniqueness in gravity and magnetic inverse problems, *Geophysics,* **36,** No. 5, 835–855.

Ander, M.E., & Huestis, S.P., 1987. Gravity ideal bodies, *Geophysics,* **52**, 1265-78.

Bhattacharyya, B.K., 1966. Continuous spectrum of the total-magnetic-field anomaly due to a rectangular prismatic body, *Geophysics,* **31**, 97-121.

Blakely, R. J., 1995. *Potential theory in gravity and magnetic applications,* Cambridge University Press.

Blakely, R.J., and Simpson, R.W., 1986. Approximating edges of source bodies from magnetic or gravity anomalies, *Geophysics,* **51,** No. 7, 1494–1498.

Boschetti, F., Dentith, M. C., & List, R. D. 1996. Inversion of seismic refraction data using Genetics Algorithms. *Geophysics,* **61**, 1715-1727**.**

Boschetti, F., Dentith, M., & List, R., 1997. Inversion of potential field data by Genetic Algorithm, *Geophysical Prospecting,*, **45**, 461-478.

Bracewell, R., 1965, *The Fourier transform and its applications,* McGraw-Hill, New York.

Hornby, P., Boschetti, F., and Horowitz, F.G., 1998, Analysis of potential field data in the wavelet domain, *Geophys. Jour. Int'l.,* (in press).

Horowitz, F.G., Hornby, P., Bone D., and Craig, M., 1996. Fast Multidimensional Interpolations, *26th Proceed., Appl. Computers Oper. Res. Minerals Indust. (APCOM) XXVI,* R.V. Ramani (ed.), Soc. Mining, Metall., & Explor. (SME), Littleton, Colorado, USA, pp. 53-56.

Huestis, S.P., & Parker, R.L., 1977. Bounding the thickness of the oceanic magnetized layer, *Journal of Geophysical Research,* **82**, 5293-303.

Isaaks, E.H. and Srivastava, R.M., 1989. *An Introduction to Applied Geostatistics.* Oxford University Press, New York, Oxford.

Journel, A.G., 1997. Deterministic geostatistics: a new visit, *Geostatistics Wollongong '96,* **1**, 292-301, E.Y. Baafi & N.A. Schofield, eds., Kluwer Academic Publishers.

Ku, C.C., & Sharp, J.A., 1983. Werner deconvolution for automated magnetic interpretation and its refinement using Marquardt's inverse modeling, *Geophysics,* **48**, 754-74.

Mathias, K., Whitley, D., Stork, C., & Kusuma, T. 1994. Staged hybrid genetic algorithm search for seismic data imaging. ICEC 1994, 356-361.

Mareschal, J.C., 1985. Inversion of potential field data in Fourier transform domain, *Geophysics,* **50,** No. 4, 685–691.

Matheron, G., 1978. Estimer et Choisir, *Fasc. 7, Cahiers du Centre de Morphologie Mathématique,* Fontainebleau, France.

Miller, H.G., and Singh, V., 1994. Semiquantitative techniques for the identification and removal of directional trends in potential field data, *Journal of Applied Geophysics,* **32,** 199–211.

Naudy, H., 1971. Automatic determination of depth on aeromagnetic profiles, *Geophysics,* **36**, 717-22.

Packard, N.H., Crutchfield, J.P., Farmer, J.D., and Shaw, R.S., 1980. Geometry from a time series, *Phys. Rev. Lett.,* **45**, 712-6.

Parker, R.L., 1974. Best bounds on density and depth from gravity data, *Geophysics,* **39**, 644-9.

Parker, R.L., 1975. The theory of ideal bodies for gravity interpretation, *Geophysical Journal of the Royal Astronomical Society,* **42**, 315-34.

Pilkington, M., and Todoeschuck, J.P., 1990. Stochastic inversion for scaling geology, *Geophys. J. Int.,* **102,** 205–217.

Pilkington, M., Gregotski, M.E., and Todoeschuck, J.P., 1994. Using fractal crustal magnetization models in magnetic interpretation, *Geophysical Prospecting,* **42,** 677–692.

Press, W. H., Vetterling, W. T., Teukolsky, S. A., & Flannely, B. P., 1992. *Numerical recipes,* 2nd ed., Cambridge University Press.

Roest, W.R., Verhoef, J., and Pilkington, M., 1992. Magnetic interpretation using the 3-D analytic signal, *Geophysics,* **57,** No. 1, 116–125.

Spector, A., and Grant, F.S., 1970. Statistical models for interpreting aeromagnetic data, *Geophysics,* **35,** 293–302.

Thompson, D.T., 1982. EULDPH: a new technique for making computer-assisted depth estimates from magnetic data, *Geophysics,* **47**, 31-7.

Vasco, D. W., Johnson, L. R., & Majer, E. L. 1993. Ensemble inference in geophysical inverse problems. *Geophysical Journal International* ,**115**, 711-728.

Werner, S. 1953. Interpretation of magnetic anomalies at sheet-like bodies. *Sveriges Geologiska Undersok, Arsbak,* **43**(6), series C, no. 508.